In situ chemical sensing in AlGaN/GaN high electron mobility transistor metalorganic chemical vapor deposition process for real-time prediction of product crystal quality and advanced process control

Soon Cho[a] and Gary W. Rubloff[b]
Department of Materials Science and Engineering and Institute for Systems Research, University of Maryland, College Park, Maryland 20742

Michael E. Aumer, Darren B. Thomson, and Deborah P. Partlow
Advanced Materials and Semiconductor Device Technology Center, Northrop Grumman Electronic Systems, Linthicum, Maryland 21090

Rinku Parikh and Raymond A. Adomaitis
Department of Chemical Engineering and Institute for Systems Research, University of Maryland, College Park, Maryland 20742

(Received 7 January 2005; accepted 14 June 2005; published 18 July 2005)

Gallium nitride and its alloys promise to be key materials for future semiconductor devices aimed at high frequency, high power electronic applications. However, manufacturing for such high performance products is challenged by reproducibility and material quality constraints that are notably higher than those required for optoelectronic applications. To this end, *in situ* mass spectrometry was implemented in AlGaN/GaN/AlN/SiC metalorganic chemical vapor deposition processes as a real-time process and wafer state metrology tool. Dynamic chemical sensing through the process cycle, carried out downstream from the wafer, revealed generation of methane and ethane reaction byproducts, as well as other residual gas species. Using the methane/ethane ratio, the GaN epilayer crystal quality was shown to be predictable in real time to a precision of 2%–5%. This was verified by postprocess x-ray diffraction using the full-width at half-maximum height of GaN on-axis (002) and off-axis (102) rocking curve peaks as a measure of crystal quality. The methane/ethane ratio may have a fundamental significance in terms of the intrinsic chemistry in that these two byproducts are speculated to reflect two different reaction pathways leading to GaN growth, namely the gas phase adduct formation route and the gas phase thermal decomposition of the precursor, respectively. The fact that lower methane/ethane ratios consistently yield better crystal quality for the GaN films suggests that the gas phase thermal decomposition pathway produces higher quality GaN growth. These results demonstrate that *in situ* mass spectrometry can be used to predict material quality during crystal growth. In turn, this offers an attractive pathway to advanced process control for GaN-based semiconductor manufacturing. © *2005 American Vacuum Society.* [DOI: 10.1116/1.1993616]

I. INTRODUCTION

In recent years, gallium-nitride (GaN)- and aluminum-gallium-nitride (AlGaN)-based materials have distinguished themselves to be key materials for future semiconductor devices aimed at high frequency and high power electronic operation.[1–3] Unlike the rapidly expanding applications for GaN technology in optoelectronics (e.g., light emitting diodes), such high performance electronic applications place greater demands on the material quality which is needed for desired device performance. However, despite the potential of these materials, currently the level of control and reproducibility in these processes are no where near that achieved in the silicon-based semiconductor manufacturing, because of the complexity of the process chemistries involved, the earlier stage of the technology's evolution, and the consequent absence of emphasis on advanced process control (APC).[4–6]

Although GaN metalorganic chemical vapor deposition (MOCVD) processes have been investigated in some depth, its intrinsic chemistry is still debated.[7–34] Typically, MOCVD of GaN and AlGaN heteroepitaxial films (as shown in Fig. 1 for example) are grown at high temperatures (e.g., up to 1100 °C) using large concentrations of H_2 (carrier) and NH_3 (N source), and relatively small concentrations of metal (group III) precursors, trimethylgallium (TMG) or trimethylaluminum (TMA). The variety of active species and reaction pathways accessible at such elevated temperatures give rise to complex parasitic reactions in the gas phase as shown in Fig. 2.[35] GaN growth is characterized by two competing reaction pathways occurring in the gas phase. The upper reaction pathway leads to form complex adduct species which further decompose to form a trimer specie before finally decomposing to form GaN on the hot wafer surface. This adduct pathway releases several molecules of CH_4 (methane)

[a]Current address: Intel Corporation; electronic mail: soon.cho@intel.com
[b]Author to whom correspondence should be addressed; electronic mail: rubloff@isr.umd.edu

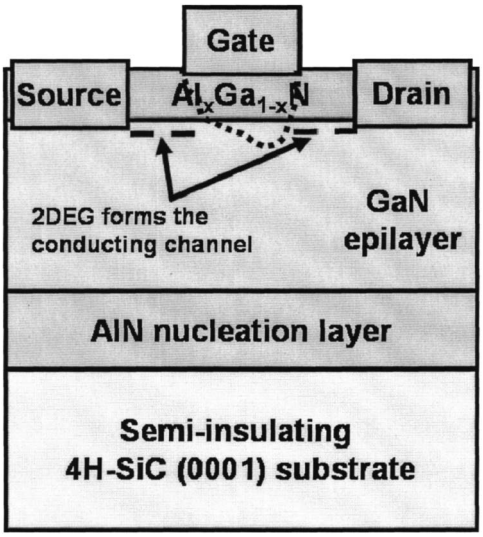

FIG. 1. Schematic representation of a HEMT based on AlGaN/GaN/AlN/SiC heterostructure as grown by the MOCVD processes discussed in this article. Not drawn to scale.

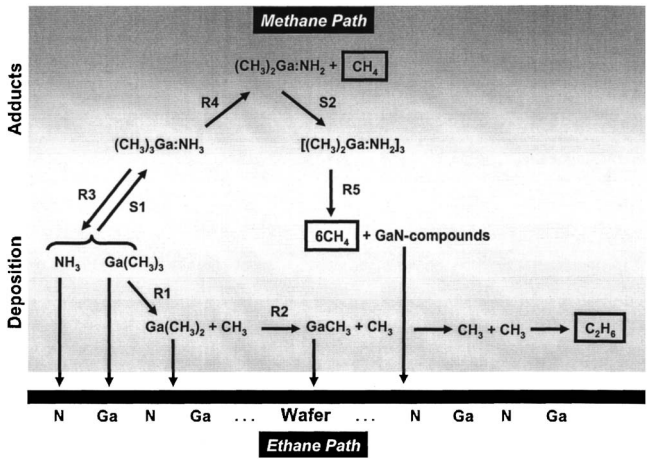

FIG. 2. Schematic representation of the proposed reaction pathways leading to GaN-based materials growth by MOCVD. The upper reaction pathway leads to complex adduct formation and reactions that result in CH_4 as its characteristic byproduct, whereas the lower reaction pathway results in thermal decomposition of the metalorganic precursor to produce C_2H_6 as its characteristic reaction byproduct. It is assumed that both pathways exist in parallel in a typical GaN growth process discussed in this dissertation and their relative contributions can be measured by the methane/ethane byproducts ratio during growth (modeling and figure by Parikh and Adomaitis).

as the reaction byproduct. On the other hand, the lower reaction pathway undergoes thermal decomposition of the metalorganic precursor releasing methyl groups that ultimately undergo recombination to form primarily C_2H_6 (ethane) as its reaction byproduct. Different groups have modeled[7–18] and observed the growth process using a variety of *in situ* monitoring techniques, including mass spectrometry,[19–28] Fourier transform infrared spectroscopy (FTIR),[28–31] laser light scattering,[31,32] ellipsometry,[33] and laser reflectometry.[34] However, controversy continues over the exact chemistry in play. Furthermore, we note that most mechanistic studies of GaN have addressed temperature (T) regimes notably below 800 °C [e.g., room temperature (RT) −800 °C for Kuech *et al.*[8–13,20,21] and RT −300 °C for Creighton *et al.*[7,19,31,32]]. In contrast, the present work focuses on the regime above 1000 °C, where electronic applications of GaN are focused.

Despite the growth chemistry that is not well understood, it is possible to achieve significant reproducibility in metrologies based on appropriate *in situ* sensors, sufficient to drive their use in APC, since this does not require mechanistic understanding of the operative chemistry. Such sensors deliver real-time process-state information for fault detection and classification (FDC) of the process and equipment (e.g., ensuring tool cleanliness with low background impurity levels, monitoring of process for real-time signatures of tool failures). In addition, it has been demonstrated that the wafer-state information derived from such real-time sensor signals can be used to provide precision metrology and real-time control of the growth process itself to achieve desired postprocess targets. These kinds of FDC and course correction activities based on *in situ* sensors have become prominent in the silicon ultralarge scale integration (ULSI) industry, which is now witnessing a widespread adoption of APC.[4–6]

Our research group at the University of Maryland has been an active contributor in these various aspects of APC, especially in the use of *in situ* chemical sensors to drive real-time wafer-state metrology and control in Si ULSI processes.[36–46] Understanding the relevant challenges currently facing the development of GaN-based processes for manufacturing in electronic applications, we have applied similar APC approaches in hopes of achieving manufacturing reproducibility and increased understanding of the process chemistry.[47–52] We have employed *in situ* mass spectrometry for real-time process sensing during the GaN MOCVD process, initially devoted to numerous FDC applications and subsequently to quantitative metrologies for predicting material quality, film thickness, etc. We report here the development of a working real-time metric (based on the methane/ethane byproducts ratio) for accurately predicting the crystal quality of the product GaN epilayer, along with the associated metrology models appropriate under various process and equipment conditions.

II. EXPERIMENTS

A. Overview of equipment and process

Experiments were carried out within a water-cooled quartz-wall reactor (custom designed) as shown schematically in Fig. 3. The reactor is ~13 liter in volume and includes a quartz liner inside a double quartz furnace wall. The system uses a commercial gas delivery system supplied by EMF. Reactants (NH_3, TMA, and TMG) with the carrier gas (H_2) were delivered through two quartz delivery tubes fused to a custom designed quartz showerhead. In particular, the metalorganic precursors (TMA and TMG) and NH_3 were kept separated in their respective delivery tubes until they reached the showerhead, at which point they intermixed uniformly within the showerhead before being delivered to the

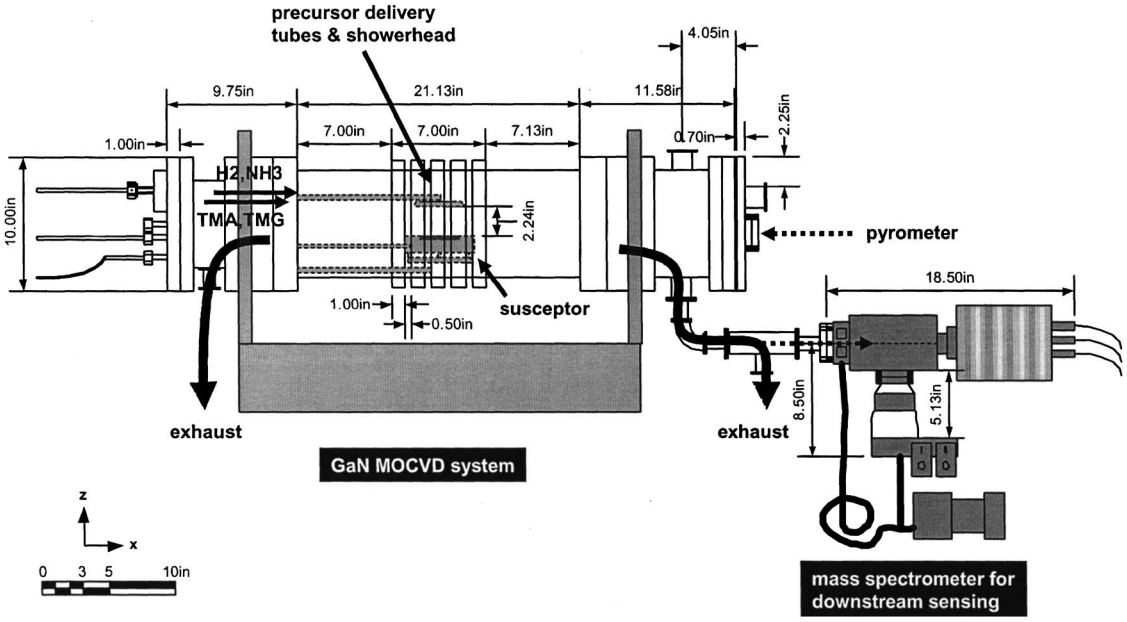

FIG. 3. Schematic representation of the 200 amu *in situ* quadrupole mass spectrometer gas sampling system (Inficon CPM™) attached to the downstream of the quartz wall reactor system for the GaN-based MOCVD processes discussed in this article.

wafer region below. Single-wafer substrate (2 in. diam semi-insulating SiC from Cree) was placed on the SiC-coated graphite susceptor. The susceptor was inductively heated at 10 kHz to provide heating for the film growth to occur on the wafer. The residual process gases were continuously pumped away through the exhaust lines located at both ends of the reactor, connected to a common rotary vane pump.

B. HEMT heterostructure growth by MOCVD

The typical process sequence used to grow GaN-based high electron mobility transistor (HEMT) heterostructures in our experiments is described in Table I. It began with 30–60 min of pregrowth room temperature reactor purge. During this period, the reactor (including the showerhead, liner, and susceptor) was purged with 25 slm of H_2 at room temperature without intentional heating of the susceptor. Once the reactor has undergone sufficiently long purge to achieve acceptable low levels of background impurities (H_2O, O_2, etc.) as monitored by the mass spectrometry, heating of the susceptor was initiated. During this step, temperature was ramped at ~1 °C/s until it reached the desired set point for growth (typically 1000–1200 °C as measured via a sapphire light pipe directed at the bottom of the susceptor). Once the temperature reached its final set point, it was maintained for an additional 5 min to outgas background impurities from both the susceptor and the liner in the presence of

TABLE I. Typical MOCVD process sequence used to grow the GaN-based HEMT heterostructure discussed in the article.

Step No.	Description	Duration	Pressure (Torr)	Temperature	Gases on
1	RT reactor purge	30–60 min	50	RT	H_2
2	*T* ramp up	20 min	50	Heating	H_2
3	High *T* reactor purge	5 min	50	At growth *T*	H_2
4	AlN growth	~15 min	50	At growth *T*	H_2, NH_3 TMA
5	GaN growth	60–90 min	50	At growth *T*	H_2, NH_3, TMG
7	AlGaN growth	1–3 min	50	At growth *T*	H_2, NH_3, TMA, TMG
8	Cooling with NH_3	1 min	Pump down (~45)	Cooling	H_2, NH_3
9	Cooling with NH_3	12 min	300	Cooling	H_2, NH_3
10	Cooling with H_2	15 min	300	Cooling	H_2
11	Cycle purge	5 min 20 s	5↔450	RT	H_2

TABLE II. Process and tool conditions used for set A runs. Larger spacing between the showerhead and susceptor was created compared to set B and C runs by the use of 0.25 in. shorter susceptor legs.

Run No.	GaN time (min)	Pressure (Torr)	Carrier gas (slm)	NH_3 (slm)	TMG (sccm)	Pyrometer T (°C)	Showerhead	Liner
G245	90	50	25	4	11	1077	F	3
G246	75	50	25	3.8	14	1082	F	9
G247	90	50	25	4.2	14	1085	F	9
G248	90	50	25	4	12	1093	F	10
G249	90	50	25	4	12	1100	F	10

the H_2 purge gas. During this high temperature reactor purge, progress in removing impurities was monitored in real time using the same mass spectrometry used for the HEMT growth sensing. In particular, the background impurity levels measured by the mass spectrometry were noted at the end of this high temperature reactor purge step for correlation to postprocess material characterization, as discussed in other publications.[47–49]

The sequence and conditions of the growth process were defined by the design of the GaN-based HEMT heterostructure required for our advanced microwave electronics application. Usually, it consisted of three layers grown on the as-received semi-insulating (resistivity $>$1E5 Ω cm) 4H-SiC(0001) substrates (2 in. diameter) as shown in Fig. 1. (1) First, a $\sim$100 nm thick AlN(0001) layer was grown to provide nucleation sites for the subsequent GaN growth and to reduce the large lattice mismatch ($\sim$3.3%) between the SiC(0001) substrate and the GaN(0001) epilayer. The thickness of the AlN layer must be carefully optimized in order to avoid GaN layer cracking (due to overly thick AlN) or poor GaN crystal quality (due to overly thin AlN). (2) Second, a $\sim$1 μm thick GaN epilayer was grown on the AlN nucleation layer. The bulk of the GaN epilayer is expected to be electrically insulating, while the two-dimensional electron gas (2DEG) near the interface of the GaN epilayer with the AlGaN cap layer forms the transistor's channel for carrier transport. In order to achieve such requirements, a number of important material parameters must be carefully optimized including the epilayer thickness, crystal quality, and impurity content, because they affect the 2DEG concentration, background carrier concentration, their mobilities, etc. (3) Finally, a 20–25 nm AlGaN cap layer was grown on the GaN epilayer to complete the heterostructure. The AlGaN cap layer composition (usually target 30%–35% Al for band gap energy of $\sim$4.0 eV) as well as the thickness (usually target 20–25 nm) must be precisely optimized and controlled for optimum electrical performance of the final device. The growth of all three layers occurred as sequential steps within the same process, and the *in situ* mass spectrometry was used to monitor the progress in real time through the entire process cycle.

Following the growth of the HEMT heterostructure at 50 Torr, the residual process gases were pumped away and the wafer was cooled under NH_3 at 300 Torr to prevent GaN decomposition. This was followed by further cooling under H_2 and cycle purge of the reactor to complete the process and remove the wafer for postprocess characterizations.

For the results discussed in this article, three sets of runs were performed. Each set was performed using significantly different tool configurations, particularly the showerhead-to-susceptor spacing and the showerhead design, as discussed in more detail at the end of the current section. For simplicity, we will denote these tool configurations by sets "A," "B," and "C" here. For all three sets, AlGaN/GaN/AlN HEMT heterostructures were grown on 2 in. semi-insulating SiC substrates as discussed already in the current section. The individual HEMT heterostructures were grown under varying process conditions (TMG flows, growth temperature, growth duration, etc.) and using different equipment configuration (showerhead, liner, etc.) as described in Tables II–IV.

Typically, the TMG flow rate and the growth temperature were varied while the total pressure, carrier gas, and NH_3 gas flow rates were maintained constant run-to-run. The process temperature set point (as measured via a sapphire light pipe directed at the bottom of the susceptor) was intentionally varied, and the actual temperature was confirmed by an independent optical pyrometer aimed at one side of the susceptor, which is reported in Tables II–IV. In addition to the two

TABLE III. Process and tool conditions used for set B runs. The showerhead to susceptor spacing was smaller than for set A runs by the use of 0.25 in. longer susceptor legs.

Run No.	GaN time (min)	Pressure (Torr)	Carrier gas (slm)	NH_3 (slm)	TMG (sccm)	Pyrometer T (°C)	Showerhead	Liner
G262	60	50	25	4	18	1106	F	9
G263	60	50	25	4	20	1115	F	11
G264	60	50	25	4	22	1130	F	11

TABLE IV. Process and tool conditions used for set C runs. The showerhead to susceptor spacing was smaller than for set A runs by the use of 0.25 in. longer susceptor legs. Also, showerheads with markedly different hole pattern were used compared to set A and B runs.

Run No.	GaN time (min)	Pressure (Torr)	Carrier gas (slm)	NH_3 (slm)	TMG (sccm)	Pyrometer T (°C)	Showerhead	Liner
G379	90	50	15	3	15	1111	G	3
G380	90	50	15	3	15	1102	G	3
G382	95	50	15	3	20	1111	G	12
G386	90	50	15	3	20	1113	G	18

types of direct temperature measurements, other indirect means to infer the actual process temperature were also employed, including measurement of the cooling water temperature exiting the reactor and the utilized rf power output.

The showerheads were made of quartz and custom-designed by one of our co-authors (R. Adomaitis) through a physically based model describing heat transfer and gas transport through the showerhead.[53] For example, showerheads "F" (used for set A and B runs) and "G" (used for set C runs) differed markedly in their hole pattern, size, and distribution. Both the showerhead and the innermost liner were removed from the reactor after each run. Showerheads were cleaned in ultrasonic KOH solution bath run-to-run, while the liners were used for ~3 runs without cleaning. On average, a showerhead could be used for ~10 runs before being replaced due to the effect of the showerhead surface roughening on film growth uniformity. Finally, the showerhead-to-susceptor spacing was intentionally varied by the use of 0.25 in. longer susceptor legs for sets B and C compared to set A.

C. Real-time *in situ* process sensing by mass spectrometry

The mass spectrometry sampling system used is shown schematically in Fig. 3. The process and residual gases were sampled directly from the reactor downstream via a 1/16 in. o.d. × 0.010 in. i.d. × 20 cm long stainless steel capillary, which resulted in a pressure drop from the process pressure of 50 Torr down to ~1 Torr behind the capillary. Most of this gas was then pumped away by a bypass differential pumping to the foreline of the diaphragm pump (backing pump for the mass spectrometer's turbomolecular pump), leaving only a small fraction of the gas to enter a 20 μm i.d. orifice into the closed ion source region of the mass spec (Inficon model CPM™, 200 amu quadrupole mass spectrometer).

By using an appropriately sized capillary-orifice combination for the gas conductance network, the sampled gas pressure was reduced from the viscous flow regime (50 Torr) to the molecular flow regime (~1 Torr). The bypass differential pumping technique enabled us to actively withdraw gases from the process through the sampling system. Both of these sampling techniques, as well as the location of the sampling capillary (i.e., within the main gas flow downstream to the growth reaction), were critical in achieving adequate response time in process sensing.

The W filament current in the closed ion source was kept at 200 μA, while the electron energy was maintained at 40 eV. This provided adequate sensitivity and minimum parasitic reactions within the closed ion source region. Electron multiplier detection was used at an acceleration voltages of 1000 V (for sets A and B) and 835 V (for set C after the electron multiplier unit was replaced) to enhance and maintain the signal-to-noise ratio run-to-run.

D. Postprocess material characterizations

The samples grown on SiC substrates as described in the preceding sections were examined using a number of post-process characterization techniques, including x-ray diffraction (XRD), x-ray reflectance (XRR), and photoluminescence (PL). In particular, the XRD was performed using a Bede D1™ system equipped with microsource capability for higher spatial resolution. Rocking curves were obtained at 81 points on an equally spaced rectangular grid over the 2 in. wafer. Full-width at half-maximum (FWHM) height of the individual rocking curves were obtained and averaged to provide a measure of the average crystal quality of the GaN epilayer. For set A runs, FWHMs were measured for both the on-axis (002) symmetric and off-axis (102) glancing exit reflections. The on-axis reflection (most commonly reported) alone is considered to be insufficient as a metric for GaN crystal quality because it is not affected by edge dislocations [i.e., the material can have large density of edge dislocations and still produce a narrow (002) peak]. However, it was found over the course of many runs that the presence of the two types of defects (edge and screw dislocations) were in general correlated (i.e., found together), and the off-axis (102) reflection therefore did not provide any additional information to that from the on-axis (002) reflection. Also, in an effort to improve our throughput, the number of points analyzed across the wafer was reduced to nine for set C runs.

III. RESULTS

A. Real-time *in situ* metrology development

In situ mass spectrometry sensing of the 50 Torr MOCVD

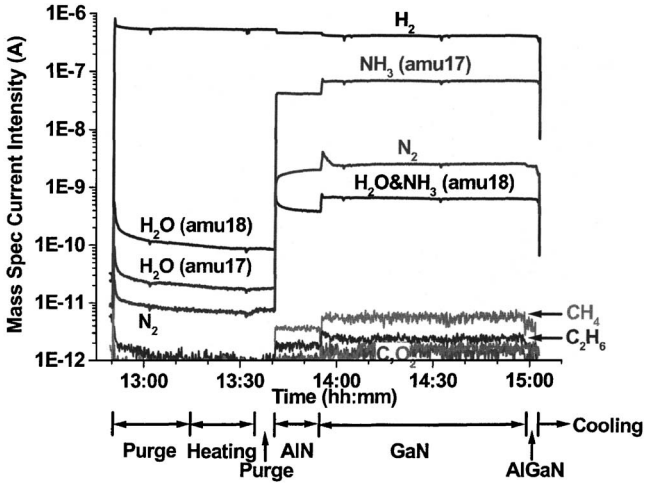

FIG. 4. *In situ* gas phase chemical signals from mass spectrometry, indicative of the dynamic gas composition downstream of the reactor as a function of process steps. The mass spectrometry current signals were acquired in real time through the entire HEMT growth process. Shown here is an example taken from run G262, for which the equipment configurations and process conditions are described in Table III.

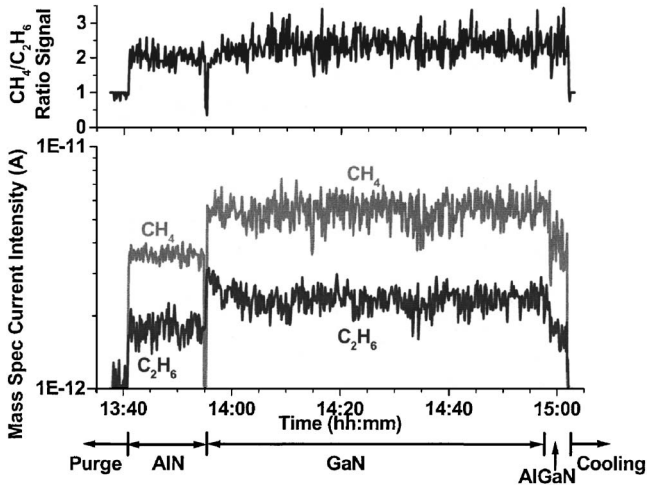

FIG. 5. *In situ* gas phase chemical signals from mass spectrometry, indicative of the dynamic gas composition downstream of the reactor as a function of process steps. Shown here are the reaction byproducts methane (at 13 amu) and ethane (at 26 amu) through the AlN, GaN, and AlGaN layer growth steps along with the corresponding methane/ethane ratio metric derived in real time. This example is taken from run G262, the same run as in Fig. 4.

growth process as described above provided dynamic, real-time gas phase chemical signals as a function of the process cycle. Figures 4 and 5 show characteristic ion current signals from H_2 (carrier gas), NH_3 (column V precursor), N_2 (fragmentation product from NH_3), H_2O (background impurity), CH_4 (reaction byproduct), C_2H_6 (reaction byproduct), C (background impurity), and O_2 (background impurity). Partial pressures for these species, reflected in the ion currents, exhibit strong time dependence throughout the entire process cycle, including the initial and final stages of the AlN, GaN, and AlGaN growth steps. This is primarily a consequence of the reactor residence time, which determines the rate at which reaction byproduct generation and reactant depletion attain steady state whenever there is a change in process chemistry (e.g., going from GaN growth to AlGaN ternary alloy growth). Virtually no column III precursors (TMA and TMG) were detectable in their original chemical form at the downstream location. This is primarily attributed to the close to complete decomposition and utilization at the extremely high growth temperature near the wafer and showerhead regions. Note also that for the reaction byproducts methane and ethane, mass peaks at 13 and 26 amu were used instead of 16 and 30 amu as one might expect (based on NIST database[54]). These values were chosen from components in the fragmentation patterns of the parent species to minimize ambiguity where mass fragments from multiple sources overlap. Specifically, this was an attempt to avoid large overlap in spectrum for the species present in the system including NH_3 (fragmentation pattern at 17, 16, 15, and 14 amu) and N_2 (fragmentation pattern at 28 and 14 amu; and parasitic ion-molecule reactions to produce N_x-H_y species at 15, 16, 29, and 30 amu). Small overlaps ($<8\%$) may have existed between methane and ethane signals knowing that additional methane can be formed inside mass spectrometer ion source as a fragment of the original ethane from the MOCVD reaction. However, with the fixed operating condition for the mass spectrometry, the minute overlap would be consistent run-to-run and therefore negligible for the purpose of our analysis described below.

Because methane and ethane are clearly the byproducts of the growth reaction of our interest, it is expected that they contain the wafer-state information indicative of deposition on the wafer, as well as the process-state information normally expected. It has already been clearly demonstrated in the past that these kinds of *in situ* sensor-based signals do indeed correlate to the wafer state in real time, in some cases with high quantitative precision that allows precision metrology[46] and subsequent control[43] of the wafer state (e.g., film thickness deposited). Moreover, in this case, assuming that each of the two byproducts come from different reaction pathways to grow the GaN-based material on the wafer (see Fig. 2), the methane/ethane ratio can be thought of as a measure of the relative contribution of each pathway for any given growth process. With this in mind, the methane/ethane ratio can be directly monitored in real time as shown in Fig. 5. Averaging the values obtained through the entire GaN growth period provides the average methane/ethane ratio metric of our interest:

$$\frac{\int \boldsymbol{S}(\mathrm{CH_4})\boldsymbol{dt}}{\int \boldsymbol{S}(\mathrm{C_2H_6})\boldsymbol{dt}}. \tag{1}$$

Next, we show how this sensor-based metric can be used to predict the product crystal quality in real time and the corresponding metrology results we have obtained in our three sets of GaN growth runs.

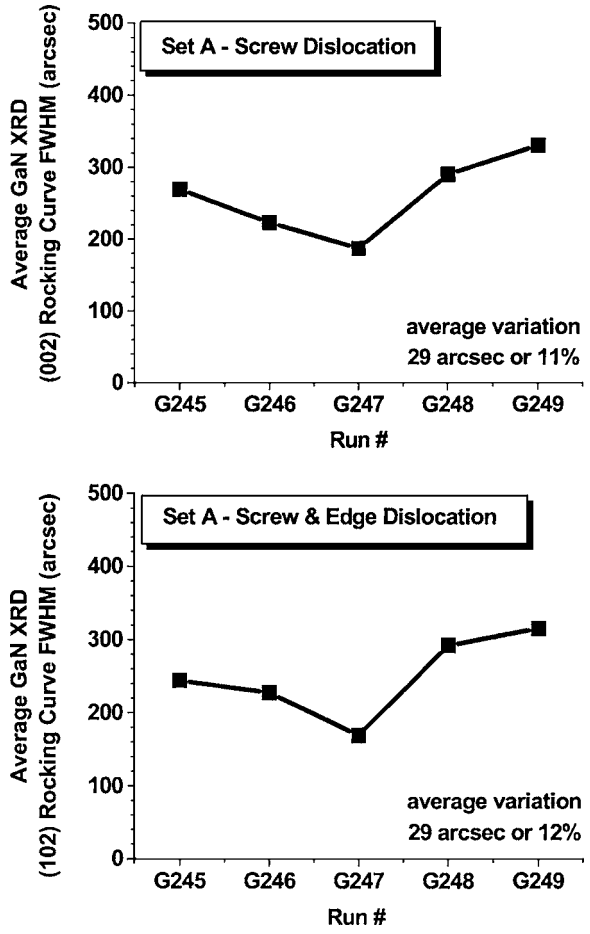

FIG. 6. Run-to-run variation in GaN epilayer crystal quality as measured by postprocess XRD shows average variation of 29 arcsec or 11%–12% for set A runs. The distortion of the (002) peak is indicative of screw dislocations, whereas that of the (102) peak is known to arise from both screw and edge dislocations.

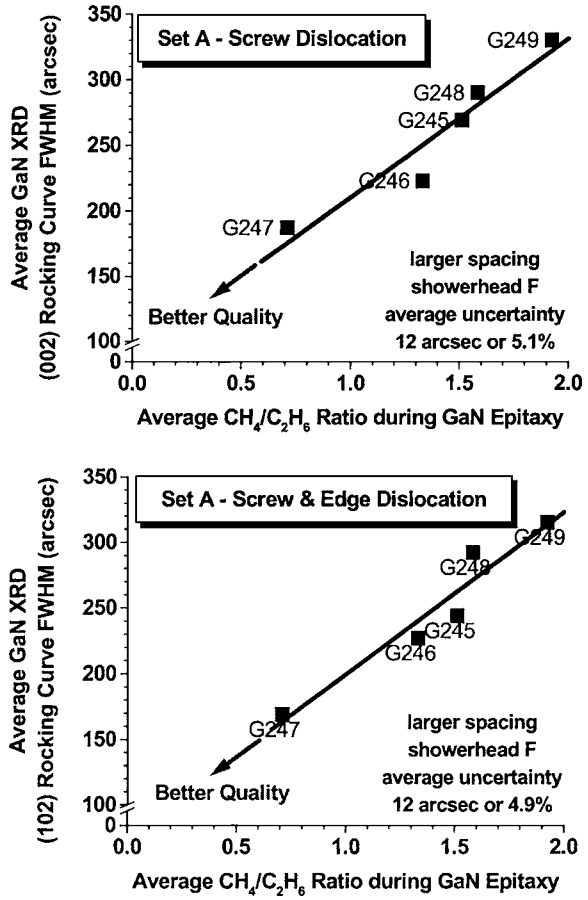

FIG. 7. Real-time prediction of GaN epilayer crystal quality during growth based on *in situ* measurement of methane/ethane byproducts ratio by mass spectrometry for set A runs. The metrology models show accuracies on the order of 5.1% average uncertainty for (002) peak and 4.9% for (102) peak, respectively. In general, narrower XRD rocking curve peaks represent better crystal quality, so in this case, it is apparent that smaller methane/ethane ratio is preferred for better GaN crystal quality.

B. Real-time prediction of GaN crystal quality and metrology

Largely due to the variation in process condition, the resulting material qualities exhibited run-to-run variability. In particular, run-to-run variation in GaN epilayer crystal quality for set A runs is shown in Fig. 6 in terms of the XRD rocking curve FWHM. As discussed in the preceding sections, distortion of the on-axis (002) reflection is considered to be due to screw dislocations, whereas the off-axis (102) reflection is affected by both screw and edge dislocations. However, both types of measurement exhibited similar trends of run-to-run variation on the order of 29 arcsec or 11%–12%.

Despite such unintentional variation in product crystal quality, we have found it can be successfully predicted in real time during growth using the methane/ethane ratio metric as discussed in the preceding section. Figure 7 shows the correlation between real-time methane/ethane ratio during growth and crystal quality as measured by postprocess XRD characterization. Linear fit to the data indicates that the correlation to the on-axis (002) reflection is accurate to within 12 arcsec or 5.1% average uncertainty, and similarly the off-axis (102) reflection to within 12 arcsec or 4.9% average uncertainty. The same results are also tabulated in Table V along with the GaN epilayer thickness information, which is calculated based on the PL interference fringe separation in the white light spectrum (Accent model RPM2000™ compound semiconductor photoluminescence system was used). In general, thickness and growth rate correlate to the resulting crystal quality of the epitaxial films in such a way that larger thickness and lower growth rate are expected to produce better crystal quality epitaxial films. However, the PL thickness information along with the average growth rate deduced from the thickness showed that our metrology models based on the methane/ethane ratio are independent of the growth rate and film thickness within the range explored.

C. Effect of changes in tool configuration

In addition to establishing a working metrology model for the set A runs as discussed above, we have also observed similar correlations (between methane/ethane ratio and crystal quality) using two significantly different tool configurations. In particular, we have explored (1) smaller vertical

TABLE V. Postprocess GaN epilayer characterization for set A runs. GaN epilayer thickness was measured by PL, from which the average growth rate could be deduced. XRD rocking curve FWHM provided a measure of epilayer crystal quality. Distortion of the on-axis (002) reflection is considered to be due to screw dislocations, whereas the off-axis (102) reflection is considered to be affected by both screw and edge dislocations. Methane/ethane ratio obtained from *in-situ* mass spectrometry serves as our real-time crystal quality prediction metric.

Run No.	Thickness by PL (μm)	Average growth rate (μm/h)	Methane/ethane ratio	XRD FWHM at (002)	XRD FWHM at (102)
G245	0.695	0.46	1.51	269	244
G246	1.354	1.08	1.33	223	227
G247	1.553	1.04	0.71	187	169
G248	1.305	0.87	1.58	290	292
G249	0.650	0.43	1.92	330	315

spacing between the showerhead and susceptor in sets B and C (Fig. 8, Table VI) and (2) significantly different showerhead design in terms of its hole pattern, size, and distribution in set C (Fig. 9, Table VII).

Overall results indicate that small methane/ethane byproduct ratios identify better GaN epilayer crystal quality, with the corresponding metrology accurate to within 2%–5% average uncertainty, depending on the tool configuration and the associated model for the different set of runs. This is confirmed by the correlation between the real-time methane/ethane ratio measured by *in situ* chemical sensing of the reaction byproducts and the postprocess GaN crystal quality measured by XRD for changes in process conditions at a fixed tool configuration. In turn, significant changes in tool configuration (i.e., the showerhead design and the spacing between showerhead and susceptor) necessitated a change in the model, but for each tool configuration a model gave a strong correlation between mass spectrometry metrology and crystal quality.

IV. DISCUSSION

A. Elements that determine metrology/control model

The metrology models developed above, based on correlation between real-time mass spectrometry measurements of methane/ethane ratios and postprocess GaN crystal quality characterization by XRD, display substantial validity (a few %) in the presence of modest intentional changes made in run-to-run process condition within each set as seen in Tables II–IV. There also existed numerous nonintentional factors within each individual set in terms of the growth conditions, which ultimately contributed to the run-to-run material quality variation but was still well described by the model.

For example, as the showerhead aged run-to-run, its surface roughened (i.e., area increased) due to bonding of materials during process and their removal during postprocess KOH cleaning; this affected the depletion of the precursor within the showerhead and therefore the film growth uniformity on the wafer. The use of different liners brought about slight variation in the showerhead-to-susceptor spacing because the showerhead was designed to rest on the horizontal

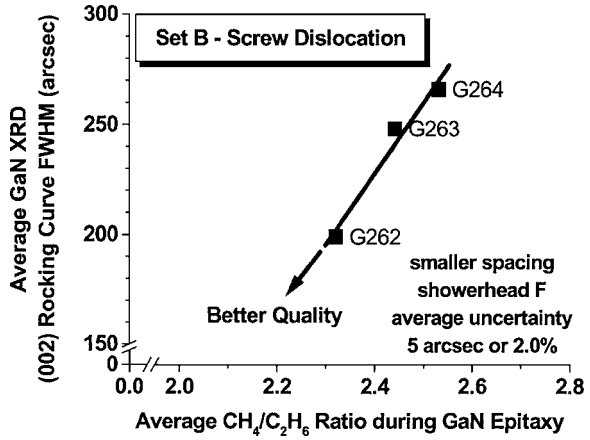

FIG. 8. Real-time prediction of GaN epilayer crystal quality during growth based on *in situ* measurement of methane/ethane byproducts ratio by mass spectrometry for set B runs. The metrology model shows accuracy on the order of 2.0% average uncertainty for the (002) peak. In general, narrower XRD rocking curve peaks represent better crystal quality, so in this case, it is apparent that smaller methane/ethane ratio is preferred for better crystal quality GaN. Identical showerhead design, but a smaller showerhead to susceptor spacing (0.25 in. less), was used compared to set A runs.

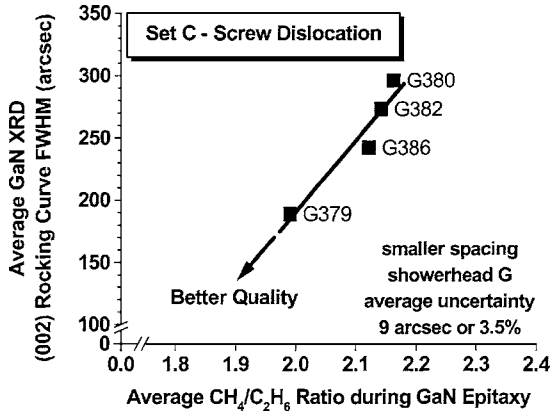

FIG. 9. Real-time prediction of GaN epilayer crystal quality during growth based on *in situ* measurement of methane/ethane byproducts ratio by mass spectrometry for set C runs. The metrology model shows accuracy on the order of 3.5% average uncertainty for the (002) peak. In general, narrower XRD rocking curve peaks represent better crystal quality, so in this case, it is apparent that smaller methane/ethane ratio is preferred for better crystal quality GaN. A completely different showerhead design, but an identical showerhead to susceptor spacing, was used compared to set B runs.

TABLE VI. Postprocess GaN epilayer characterization for set B runs. GaN epilayer thickness was measured by PL, from which the average growth rate could be deduced. XRD rocking curve FWHM provided a measure of epilayer crystal quality. Methane/ethane ratio obtained from *in-situ* mass spectrometry serves as our real-time crystal quality prediction metric.

Run No.	Thickness by PL (μm)	Average growth rate (μm/h)	Methane/ethane ratio	XRD FWHM at (002)
G262	1.197	1.20	2.32	199
G263	1.449	1.45	2.44	248
G264	1.173	1.17	2.53	266

TABLE VII. Postprocess GaN epilayer characterization for set C runs. GaN epilayer thickness was measured by PL, from which the average growth rate could be deduced. XRD rocking curve FWHM provided a measure of epilayer crystal quality. Methane/ethane ratio obtained from *in-situ* mass spectrometry serves as our real-time crystal quality prediction metric.

Run No.	Thickness by PL (μm)	Average growth rate (μm/h)	Methane/ethane ratio	XRD FWHM at (002)
G379	0.860	0.57	2.01	189
G380	0.805	0.54	2.16	296
G382	0.925	0.58	2.17	273
G386	1.083	0.72	2.12	242

crossbar built into the liner itself, whose position unintentionally varied to within the glass fabrication error of <0.125 in. This would have affected the temperature and chemistry within the showerhead positioned directly above the hot susceptor. In fact, variability observed in the run-to-run sensing data motivated a reactor design modification to eliminate the liner as a source of such variability for future runs. These types of influences on the gas phase chemistry during the process are expected to manifest in terms of the final material quality such as the crystal quality. Finally, conditions of the underlying AlN nucleation layer and SiC substrate were inconsistent run-to-run, which would have influenced the GaN epilayer grown over them. This has been proven through our routine XRD wafer mapping, where the original defects within the SiC substrate could indeed translate to undesirable defects within the AlN and GaN layers grown over them, unless steps were taken during the AlN layer growth to minimize their effect.[51]

Despite all of these intentional and nonintentional sources of variability that lead to run-to-run variations in the process environment and resulting material quality, results show that a single model developed using one tool configuration provides quantitative predictability of crystal quality over a reasonable range of process conditions. However, the models indicate strong dependence on the tool configuration parameters such as the showerhead-to-susceptor spacing and the showerhead design. These points are illustrated clearly in Fig. 10. The model relating mass spectrometry predictors of crystal quality and actual XRD measures of crystal quality changes significantly with changes in tool configuration. However, once the tool configuration is fixed, the associated model transforms the mass spectrometry measurement into an effective predictor of material quality (to a few % precision).

B. Prognosis for applications

Even though the XRD rocking curve data are only supposed to reflect a qualitative or semiquantitative measure of a material's crystal quality, such a correlation as seen here between real-time wafer-state metric based on sensors and postprocess product quality can be extremely useful from the viewpoints of both development and manufacturing.

The methane/ethane ratio offers an extremely useful metric that can be quickly utilized to identify process conditions that optimize product crystal quality. With GaN technologies still in development, this is extremely useful. For instance, a single design of experiment (DOE), containing multiple short period ($\sim$30 s) GaN growth steps within to explore a wide range of process conditions (in terms of temperature, pressure, flow rates, gas composition, etc.), may be performed on a semi-insulating SiC with a usual AlN nucleation layer. The average methane/ethane ratio resulting from each individual GaN growth step can be monitored and recorded in real time. Knowing that lower methane/ethane ratio will have a greater chance of producing better GaN crystal quality, an optimal window of process condition can be selected and employed in subsequent real HEMT heterostructure growth runs. This offers a systematic methodology to improve/tune GaN-based processes with drastically reduced turnaround time and cost.

Furthermore, since the metric is based on real-time *in situ* metrology, it can be exploited for real-time control of the MOCVD growth process in the context of APC. In one sce-

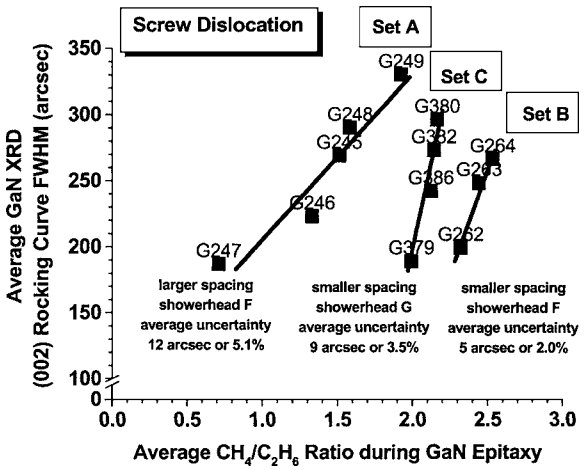

FIG. 10. Crystal quality prediction models for three different tool configurations in terms of the showerhead to susceptor spacing (larger versus smaller spacing) and the showerhead design (F versus G). It is apparent that the critical variables giving rise to a set of different metrology models are the tool configuration parameters (the showerhead-to-susceptor spacing and the specific showerhead design), not the small changes made, within each set, in temperature, gas flow rates, composition, liners, etc. Therefore, we conclude that once we define the tool configurations/geometries for our processes, we are practically defining the elements that determine the metrology/control model.

nario, the mass spectrometry signature can be employed for fault detection, identifying in real time wafers for which material quality may be degraded and triggering corrective actions ranging from more in-depth characterization to debugging and repair of equipment. Such FDC approaches have already been widely adopted in the Si ULSI industry as discussed in Sec. I.

In another scenario, the real-time mass spectrometry predictors of material quality may be employed for course correction. If an appropriate process parameter, or a set of parameters, can be identified which can improve material quality as reflected in the methane/ethane ratio, then drift in this ratio could be compensated in real time. Implementing DOEs as discussed already in the current section may aid in revealing the most appropriate and effective process parameters for this purpose. Such real-time course correction could provide significant advantage in terms of achieving reproducibility and yield by minimizing the number of scrap wafers and wasted runs due to unacceptable GaN crystal quality. Consequent cost reduction could be large, considering the irreproducibility and drift levels in the current GaN technology as well as the high per wafer materials cost in GaN-based manufacturing.

C. Implications in terms of intrinsic chemistry

One of the advantages of the foregoing application of real-time chemical sensing and metrology for manufacturing process control is that it does not require a complete understanding of the intrinsic chemistry, and can be exploited readily. Therefore, the current debate over the relevant reaction pathway and the parasitic reactions does not seem to be a major bottleneck in GaN-based technology and manufacturing for now. However, in the long run, better understanding of fundamental mechanisms will no doubt help in terms of being able to optimize process conditions, and materials and device performance.

As discussed in Sec. I, current understanding of the GaN-based MOCVD process suggests there are two competing reaction pathways, i.e., the adduct formation route and the thermal decomposition route, both occurring in the gas phase. Prior investigations have focused on significantly lower temperature regimes (RT $-800\ ^\circ$C) than those treated here for electronic applications ($>1000\ ^\circ$C). Modeling work performed within our research group[35] indicates that the operative process chemistry changes significantly with variations in reactor operating parameters, particularly in terms of the relative contributions of the two different reaction pathways. For example, increase in chamber pressure enhances the adduct formation route and ultimately increases the amount of methane because this reaction is given by a bimolecular collision rate expression. Additionally, as the temperature is raised, both reaction routes may occur in parallel. For additional details, refer to Ref. 35.

Currently, a debate exists over which reaction pathway is responsible for GaN growth. One side believes that GaN growth is dominated by the upper route mainly through the formation of the cyclic trimer species.[8–10,16] The other side of the argument believes that GaN growth is dominated by the lower route through pyrolysis of the metalorganic precursor.[14,25] Essentially, both reaction pathways are possible, and the selectivity between the two reaction rate parameters are significantly influenced by the choice of reactor operating conditions, residence time in heated zones, degree of precursor mixing as determined by the design of the gas delivery system, reactor geometry, and the choice of reaction rate parameters.[35]

The methane/ethane ratio metric can be monitored, since ethane is assumed to be produced as a byproduct of the thermal decomposition route and not the adduct route. We plan further exploratory investigations to elucidate these issues related to the intrinsic process chemistry. It is also acknowledged that our studies are rather limited to specific process/tool conditions geared towards electronic applications of GaN (i.e., high $T>1000\ ^\circ$C, semi-insulating SiC substrate). In any case, all of our results to date indicate that the direct decomposition of the metalorganic precursor leads to better crystal quality than does the adduct pathway. However, it is acknowledged that our studies are focused on specific process/tool conditions geared towards electronic applications of GaN (e.g., $>1000\ ^\circ$C, semi-insulating SiC substrate).

D. Other material quality metrics of importance

In developing real-time, *in situ* methods for sensing, metrology, and control as reported here, we have focused on crystalline perfection characterized by XRD as the measure of material quality. However, this is certainly not the only measure of a material's quality: other relevant and important measures include PL, XRR, sheet resistance, Hall effect measurement, secondary ion mass spectrometry, etc. We have routinely examined our HEMT heterostructure films using these postprocess techniques. In particular, the same x-ray machine (Bede D1™ system) was also used to measure the thickness of the AlGaN cap layer ($\sim$20 nm), where the separation of interference fringes in the XRR mode gave information on the thin layer's thickness. Usually prior to all other types of characterization, PL was performed to obtain various measures of material quality, such as the band-edge and deep-level intensities, thickness of the GaN epilayer ($\sim 1\ \mu$m), and the composition of the AlGaN cap layer. In addition, due to the nature of our application in high frequency and power electronics, electrical measurements such as sheet resistance and Hall effect measurement for carrier mobility are also important.

Optimization of all of these postprocess material quality metrics is important as well. Based on our results to date, we foresee analogous applications of real-time, *in situ* sensing for metrology and APC tied to these material performance metrics. For example, mass spectrometry may be useful for AlGaN cap layer thickness as a real-time course correction application,[50] while the correlation of mass spectrometry signals to band-edge and/or deep-level PL may provide another approach to FDC.[49] Results along these lines will be discussed in separate publications.

V. CONCLUSIONS

In situ mass spectrometry sensing was implemented in 50 Torr AlGaN/GaN/AlN/SiC HEMT heterostructure growth processes in order to enhance and control process reproducibility, and to achieve better understanding of the intrinsic chemistry involved. Dynamic chemical sensing through the process cycle, carried out downstream from the wafer, revealed generation of methane and ethane reaction byproducts in real time, in addition to other residual gas species present in the process. Using the methane/ethane ratio, GaN epilayer crystal quality was shown to be predictable in real time during growth with quantitative precision of 2%–5%. This was verified by postprocess x-ray diffraction using the full-width at half-maximum height of GaN on-axis (002) and off-axis (102) rocking curve peaks as a measure of crystal quality. The same correlation was shown using three different tool configurations with combinations of different showerhead designs and varied spacing between showerhead and susceptor.

The correlation shown here between the real-time wafer-state metric based on sensors and postprocess product quality represents a significant advantage for GaN technology development in that it can be utilized in design of experiments to quickly identify the optimal range of process conditions for best product quality. This offers a systematic methodology to improve/tune GaN-based manufacturing processes with drastically reduced turn-around time and cost. The results also promise benefit to manufacturing process control in the growth of GaN-based heterostructures, both in terms of fault detection and potential course correction as well, opening the door to the efficiencies and cost benefits of advanced process control.

These results have further implications in terms of the intrinsic chemistry in that the two byproducts, methane and ethane, are known to be associated with the two different reaction pathways leading to GaN growth (i.e., gas phase adduct formation route and gas phase thermal decomposition of precursor, respectively). The fact that smaller methane/ethane ratio during process consistently yields better crystal quality GaN film suggests that the reaction pathway involving direct thermal decomposition of the metalorganic precursor produces higher quality GaN material than does the adduct pathway.

In summary, this work shows significant benefit from *in situ* mass spectrometry as a real-time process and wafer state sensor. Its ability to identify signatures of wafer state changes correlated with material quality opens the door to expedited development, manufacturing process control, and enhanced understanding of fundamental mechanisms.

ACKNOWLEDGMENTS

The authors are grateful for a close research partnership with, and financial support from, the Northrop Grumman Corporation. They also appreciate continuing interaction and technical support from Inficon, Inc., particularly R. Ellefson and L. Frees. Inficon is a supplier of mass spectrometric sensors for process control applications in semiconductor manufacturing processes.

[1] L. F. Eastman and U. K. Mishra, IEEE Spectrum **5**, 28 (2002).
[2] U. K. Mishra, P. Parikh, and Y. Wu, Proc. IEEE **90**, 1022 (2002).
[3] R. J. Trew, Proc. IEEE **90**, 1032 (2002).
[4] T. Sonderman, M. Miller, and C. Bode, Future Fab International **12**, 119 (2002).
[5] S. W. Butler, J. Vac. Sci. Technol. B **13**, 1917 (1995).
[6] G. G. Barna, B. V. Eck, and J. W. Hosch, *Handbook of Silicon Semiconductor Metrology* (Marcel Dekker, Inc., Austin, TX, 2001), pp. 601–678.
[7] J. R. Creighton, J. Electron. Mater. **31**, 1337 (2002).
[8] J. Sun, J. M. Redwing, and T. F. Kuech, J. Electron. Mater. **29**, 2 (2000).
[9] J. Sun, J. M. Redwing, and T. F. Kuech, Phys. Status Solidi A **176**, 693 (1999).
[10] S. A. Safvi, J. M. Redwing, M. A. Tischler, and T. F. Kuech, J. Electrochem. Soc. **144**, 1789 (1997).
[11] D. D. Koleske, A. E. Wickenden, R. L. Henry, M. E. Twigg, J. C. Culbertson, and R. J. Gorman, MRS Internet J. Nitride Semicond. Res. **4S1**, G3.70 (1999).
[12] D. D. Koleske, A. E. Wickenden, R. L. Henry, M. E. Twigg, J. C. Culbertson, and R. J. Gorman, Appl. Phys. Lett. **73**, 2018 (1998).
[13] D. D. Koleske, A. E. Wickenden, R. L. Henry, W. J. DeSisto, and R. J. Gorman, J. Appl. Phys. **84**, 1998 (1998).
[14] R. P. Pawlowski, C. Theodoropoulos, A. G. Salinger, T. J. Mountziaris, H. K. Moffat, J. N. Shadid, and E. J. Thrush, J. Cryst. Growth **221**, 622 (2000).
[15] A. Tachibana, O. Makino, S. Tanimura, H. Tokunaga, N. Akutsu, and K. Matsumoto, Phys. Status Solidi A **176**, 699 (1999).
[16] T. G. Mihopoulos, V. Gupta, and K. F. Jensen, J. Cryst. Growth **195**, 733 (1998).
[17] C. H. Chen, H. Liu, D. Steigerwald, W. Imler, C. P. Kuo, M. G. Craford, M. Ludowise, S. Lester, and J. Amano, J. Electron. Mater. **25**, 1004 (1996).
[18] Y. S. Hiraoka and M. Mashita, J. Cryst. Growth **136**, 94 (1994).
[19] M. E. Bartram and J. R. Creighton, MRS Internet J. Nitride Semicond. Res. **4S1**, G3.68 (1999).
[20] A. Thon and T. F. Kuech, Appl. Phys. Lett. **69**, 55 (1996).
[21] S. A. Safvi, A. Thon, J. M. Redwing, M. E. Tischler, and T. F. Kuech, in *Proceedings of the Thirteenth International Conference on Chemical Vapor Deposition*, edited by T. M. Besmann, M. D. Allendorf, McD. Robinson, and R. K. Ulrich (Electrochemical Society, Pennington, NJ, 1996), pp. 119–124.
[22] U. Bergmann, V. Reimer, and B. Atakan, Phys. Chem. Chem. Phys. **1**, 5593 (1999).
[23] U. Bergmann, V. Reimer, and B. Atakan, Phys. Status Solidi A **176**, 719 (1999).
[24] T. Li, R. P. Campion, C. T. Foxon, S. A. Rushworth, and L. M. Smith, J. Cryst. Growth **251**, 499 (2003).
[25] D. Sengupta, J. Phys. Chem. B **107**, 291 (2003).
[26] J. Schafer, A. Simons, J. Wolfrum, and R. A. Fischer, Chem. Phys. Lett. **319**, 477 (2000).
[27] C. A. Larsen, N. I. Buchan, S. H. Li, and G. B. Stringfellow, J. Cryst. Growth **102**, 103 (1990).
[28] M. J. Almond, M. G. B. Drew, C. E. Jenkins, and D. A. Rice, J. Chem. Soc. Dalton Trans. **1992**, 5 (1992).
[29] M. J. Almond, C. E. Jenkins, and D. A. Rice, J. Organomet. Chem. **439**, 251 (1992).
[30] S. H. Kim, H. S. Kim, J. S. Hwang, J. G. Choi, and P. J. Chong, Chem. Mater. **6**, 278 (1994).
[31] J. R. Creighton, G. T. Wang, W. G. Breiland, and M. E. Coltrin, J. Cryst. Growth **261**, 204 (2004).
[32] J. R. Creighton, W. G. Breiland, M. E. Coltrin, and R. P. Pawlowski, Appl. Phys. Lett. **81**, 2626 (2002).
[33] M. Losurdo, P. Capezzuto, and G. Bruno, Phys. Status Solidi A **176**, 733 (1999).
[34] A. Rebey, T. Boufaden, and B. E. Jani, J. Cryst. Growth **203**, 12 (1999).
[35] R. P. Parikh and R. A. Adomaitis, J. Cryst. Growth (submitted).
[36] L. L. Tedder, G. W. Rubloff, I. Shareef, M. Anderle, D.-H. Kim, and G. N. Parsons, J. Vac. Sci. Technol. B **13**, 1924 (1995).
[37] L. L. Tedder, G. W. Rubloff, B. F. Cohaghan, and G. N. Parsons, J. Vac. Sci. Technol. A **14**, 267 (1996).

[38]A. I. Chowdhury, W. W. Read, G. W. Rubloff, L. L. Tedder, and G. N. Parsons, J. Vac. Sci. Technol. B **15**, 127 (1997).
[39]G. Lu, L. L. Tedder, and G. W. Rubloff, J. Vac. Sci. Technol. B **17**, 1417 (1999).
[40]T. Gougousi, Y. Xu, J. N. Kidder, Jr., G. W. Rubloff, and C. R. Tilford, J. Vac. Sci. Technol. B **18**, 1352 (2000).
[41]L. Henn-Lecordier, J. N. Kidder, Jr., G. W. Rubloff, C. A. Gogol, and A. Wajid, J. Vac. Sci. Technol. A **19**, 621 (2001).
[42]R. Sreenivasan, T. Gougousi, Y. Xu, J. Kidder, Jr., E. Zafiriou, and G. W. Rubloff, J. Vac. Sci. Technol. B **19**, 1931 (2001).
[43]Y. Xu, T. Gougousi, L. Henn-Lecordier, Y. Liu, S. Cho, and G. W. Rubloff, J. Vac. Sci. Technol. B **20**, 2351 (2002).
[44]L. Henn-Lecordier, J. N. Kidder, Jr., G. W. Rubloff, C. A. Gogol, and A. Wajid, J. Vac. Sci. Technol. B **21**, 1055 (2003).
[45]S. Cho, L. Henn-Lecordier, A. Singhal, Y. Xu, Y. Liu, J. N. Kidder, Jr., and G. W. Rubloff, in *AEC/APC Symposium XV*, edited by International Sematech (International Sematech, Austin, TX, 2003).
[46]S. Cho, L. Henn-Lecordier, Y. Liu, and G. W. Rubloff, J. Vac. Sci. Technol. B **22**, 880 (2004).
[47]S. Cho, G. W. Rubloff, M. E. Aumer, D. B. Thomson, and D. P. Partlow, Presented at the AVS 50th International Symposium, Baltimore, MD, 3 November 2003 (unpublished).
[48]S. Cho, G. W. Rubloff, M. E. Aumer, D. B. Thomson, and D. P. Partlow, Presented at the MRS Fall Meeting, Boston, MA, 1 December 2003 (unpublished).
[49]S. Cho, G. W. Rubloff, M. E. Aumer, D. B. Thomson, and D. P. Partlow, J. Vac. Sci. Technol. B **23** (2005).
[50]S. Cho, D. S. Janiak, G. W. Rubloff, M. E. Aumer, D. B. Thomson, and D. P. Partlow, J. Vac. Sci. Technol. B (submitted).
[51]M. E. Aumer, D. B. Thomson, D. P. Partlow, R. C. Clarke, S. Cho, G. W. Rubloff, and R. A. Adomaitis, Presented at the AVS 50th International Symposium, Baltimore, MD, 2 November 2003 (unpublished).
[52]M. E. Aumer, D. B. Thomson, D. Partlow, S. Cho, G. Rubloff, R. Adomaitis, G. Henry, G. Augustine, and R. C. Clarke, presented at the MRS Fall Meeting, Boston, MA, 1 December 2003 (unpublished).
[53]B. D. Hoffman and R. A. Adomaitis, IEEE Trans. Semicond. Manuf.(submitted).
[54]NIST Chemistry Webbook Database ⟨http://webbook.nist.gov/chemistry⟩.